SCIENTIFIC REPORTS

OPEN

SUBJECT AREAS:
COMPUTATIONAL BIOPHYSICS
CALCIUM SIGNALLING

Received
29 July 2014

Accepted
24 December 2014

Published
23 January 2015

Correspondence and requests for materials should be addressed to J.S. (jianweishuai@xmu.edu.cn)

Optimal microdomain crosstalk between endoplasmic reticulum and mitochondria for Ca^{2+} oscillations

Hong Qi[1], Linxi Li[1] & Jianwei Shuai[1,2,3]

[1]Department of Physics, Xiamen University, Xiamen 361005, China, [2]State Key Laboratory of Cellular Stress Biology, Innovation Center for Cell Biology, Xiamen University, Xiamen 361005, China, [3]Fujian Provincial Key Laboratory of Theoretical and Computational Chemistry, Xiamen University, Xiamen 361005, China.

A Ca^{2+} signaling model is proposed to consider the crosstalk of Ca^{2+} ions between endoplasmic reticulum (ER) and mitochondria within microdomains around inositol 1, 4, 5-trisphosphate receptors (IP_3R) and the mitochondrial Ca^{2+} uniporter (MCU). Our model predicts that there is a critical IP_3R-MCU distance at which 50% of the ER-released Ca^{2+} is taken up by mitochondria and that mitochondria modulate Ca^{2+} signals differently when outside of this critical distance. This study highlights the importance of the IP_3R-MCU distance on Ca^{2+} signaling dynamics. The model predicts that when MCU are too closely associated with IP_3Rs, the enhanced mitochondrial Ca^{2+} uptake will produce an increase of cytosolic Ca^{2+} spike amplitude. Notably, the model demonstrates the existence of an optimal IP_3R-MCU distance (30–85 nm) for effective Ca^{2+} transfer and the successful generation of Ca^{2+} signals in healthy cells. We suggest that the space between the inner and outer mitochondria membranes provides a defense mechanism against occurrences of high $[Ca^{2+}]_{Cyt}$. Our results also hint at a possible pathological mechanism in which abnormally high $[Ca^{2+}]_{Cyt}$ arises when the IP_3R-MCU distance is in excess of the optimal range.

The calcium ion (Ca^{2+}) is a ubiquitous intracellular signal controlling diverse cellular functions, such as muscle cell contraction, neurotransmitter release from neurons and astrocytes, metabolic processes, egg activation, and cell maturation, differentiation and death[1]. Ca^{2+} signals commonly appear as repetitive spikes of cytosolic Ca^{2+} concentration ($[Ca^{2+}]_{Cyt}$), with signaling information encoded in the frequency, amplitude and duration of these oscillations[2]. The complex spatial-temporal profiles of $[Ca^{2+}]_{Cyt}$ depend heavily on the endoplasmic reticulum (ER) and mitochondria[3] which act as the two major intracellular Ca^{2+} stores.

While it has been widely accepted that the inositol 1, 4, 5-trisphosphate receptors (IP_3R) function as Ca^{2+} release channels on the ER membrane[1], mitochondria were previously considered only to function as Ca^{2+}-sinks under pathological conditions when there is an abnormally high cellular Ca^{2+}[3]. This view on mitochondria began to change in the 1990s with two landmark studies demonstrating that non-pathological elevations of $[Ca^{2+}]_{Cyt}$ are accompanied by a marked rise of mitochondrial matrix Ca^{2+} concentrations ($[Ca^{2+}]_{Mt}$)[4] and that $[Ca^{2+}]_{Mt}$ responds dynamically to physiological oscillations of $[Ca^{2+}]_{Cyt}$[5]. Experimental observations indicated that mitochondria can accumulate Ca^{2+} through the mitochondrial Ca^{2+} uniporter (MCU) which is located on the inner mitochondrial membrane (IMM)[6]. In despite of its low Ca^{2+} affinity, the MCU is exposed to a high $[Ca^{2+}]_{Cyt}$ generated in microdomain around the channel pore of open IP_3Rs[7,8], thus even when global $[Ca^{2+}]_{Cyt}$ is low a high value of $[Ca^{2+}]_{Mt}$ may be observed. As a result, mitochondria can serve as buffers of cytoplasmic Ca^{2+} under both pathological and non-pathological conditions.

Although it is now generally believed that mitochondria function as a dynamic Ca^{2+} sequestration system to shape cytosolic Ca^{2+} oscillations, and therefore regulate many physiological processes[6], the detailed mechanism underlying how mitochondria influence global Ca^{2+} signals remains elusive. Contradictory mechanisms have been suggested on how mitochondrial Ca^{2+} uptake regulates IP_3R activity, including up-regulation[9–11], down-regulation[12,13] and complete independence[14]. Furthermore, although mitochondrial Ca^{2+} uptake via MCU depends primarily on the spacing between the ER and mitochondria[15], the working distance between the two organelles remains unclear due to the complexity of the intracellular environment and the lack of spatial resolution in the experimental observations. Indeed, the existing estimates of the distances between the ER and mitochondria vary hugely, from less than 10 nm to more than 200 nm[16]. A recent paper published in

PNAS[17] even argued that the mitochondria may not act as a significant dynamic buffer of cytosolic Ca^{2+} under physiological conditions.

Computational models provide a valuable tool for understanding of the mechanisms underlying Ca^{2+} signal transduction[18] and the dynamics of Ca^{2+} release from the ER has been extensively modeled[19–23]. Some models only focused on mitochondrial Ca^{2+} dynamics[24,25]. Dash and co-workers developed a detailed kinetic model for MCU to match published data sets on mitochondrial Ca^{2+} uptake[25]. However, the involvement of both the ER and mitochondria in Ca^{2+} dynamics has only been considered in a limited number of models[18,26–30]. In the earlier models[18,26], it was postulated that the MCU substantially sequesters Ca^{2+} when $[Ca^{2+}]_{Cyt} < 1$ μM, in contrast to experimental evidence that the MCU actually sequesters Ca^{2+} in the range of 10–20 μM[3,31]. Dupont et al.[28] modeled the effect of Hint2, a mitochondrial protein, on cytosolic Ca^{2+} dynamics in hepatocytes. However, in these models the maximum value of ER luminal $[Ca^{2+}]$ ($[Ca^{2+}]_{ER}$) is in the order of several to several tens of μM, deviating drastically from most of the measured figures of 100–900 μM[32], and the value of $[Ca^{2+}]_{Mt}$ was also significantly underestimated. More importantly, except the model proposed by Szopa et al.[29], none of them take into account the high $[Ca^{2+}]_{Cyt}$ microdomain, which is critical for mitochondrial Ca^{2+} signaling. The model considered by Szopa et al.[29] is a modification of the model from ref. 26, analyzing the influence of microdomain on the period and shape of calcium oscillations. They supposed that MCU sense elevated Ca^{2+} concentration which is directly equal to that in ER[29]. This assumption is incoherent with the experimental observation that $[Ca^{2+}]_{Cyt}$ in microdomain is about several tens of μM, which is about 10-fold higher than that in the bulk cytosol[7] and about 10-fold lower than that in ER[32]. Thus, there is a lack of model to quantitatively investigate how the crosstalk between the ER and mitochondria controls Ca^{2+} signaling.

Here we consider a more realistic model to investigate the role of mitochondria in Ca^{2+} signaling to couple the ER and mitochondria based on the Ca^{2+} microdomain. A cytosolic microdomain is specifically considered in order to discuss the MCU dynamics and so each MCU specifically responds to the local high Ca^{2+} concentration in microdomain generated by a cluster of IP_3Rs. Our results demonstrate the critical role of mitochondrial Ca^{2+} uptake in modulating IP_3R-released Ca^{2+} signaling. We show that the location of the MCU relative to IP_3Rs is a key determinant for modulating Ca^{2+} signals. There is a critical IP_3R-MCU distance at which 50% of the ER-released Ca^{2+} is taken up by mitochondria and that mitochondria modulate Ca^{2+} signals differently when outside of this critical distance. When the IP_3R-MCU distance is greater than the critical distance mitochondrial Ca^{2+} uptake stimulates ER-Ca^{2+} release by rapidly reducing the amplitude of the $[Ca^{2+}]_{Cyt}$ signal within the microdomain and suppressing the inhibition dynamics of high $[Ca^{2+}]_{Cyt}$ on IP_3R. However, when the distance is less than the critical distance, mitochondrial Ca^{2+} uptake demonstrates a different effect on IP_3R dynamics. Initially strong mitochondrial uptake forces $[Ca^{2+}]_{Cyt}$ to a low level, thus preventing the strong activation dynamics of $[Ca^{2+}]_{Cyt}$ on IP_3R. This leads to strong IP_3R inhibition on the decay of subsequent $[Ca^{2+}]_{Cyt}$ spikes. Thus, our model predicts that when MCU are too closely associated with IP_3Rs, the enhanced mitochondrial Ca^{2+} uptake will produce an increase of cytosolic Ca^{2+} spike amplitude. As a result, there is an optimal spacing about 30–85 nm between the ER and mitochondria for generation of experimentally observed Ca^{2+} oscillations in living cells.

Modelling coupled ER and mitochondria Ca^{2+} dynamics

A "closed" cell model, which does not include Ca^{2+} exchange between cytosol and external medium through the plasma membrane, is considered to investigate the coupling effects between the ER and mitochondria on Ca^{2+} signaling (Fig. 1(a)). As a result, the model has three compartments: cytosol (Cyt), ER and mitochondria (Mt). As shown in Fig. 1(a), the dynamics of the free $[Ca^{2+}]$ in these compartments is determined by the Ca^{2+} fluxes from various channels and pumps and by buffering processes with various Ca^{2+} binding proteins (BP), given by,

$$\frac{d[Ca^{2+}]_{Cyt}}{dt} = j_{ER}^{out} - j_{ER}^{in} + j_{Mt}^{out} - j_{Mt}^{in} + j_{CaCyt}, \quad (1)$$

$$\frac{d[Ca^{2+}]_{ER}}{dt} = V_{Cyt}/V_{ER}(j_{ER}^{in} - j_{ER}^{out}) + j_{CaER}, \quad (2)$$

$$\frac{d[Ca^{2+}]_{Mt}}{dt} = V_{Cyt}/V_{Mt}(j_{Mt}^{in} - j_{Mt}^{out}) + j_{CaMt}. \quad (3)$$

Here $[Ca^{2+}]$ represents the free $[Ca^{2+}]$, V the volume of three compartments, j^{in} the Ca^{2+} flux from outside to inside, and j^{out} the opposite flux. The three terms j_{Ca} represent Ca^{2+} dissociated from the BP.

In each compartment, Ca^{2+} can be buffered by various BPs. The kinetics between free Ca^{2+} and BP is described by a simple chemical reaction

$$Ca_i + BP_i \underset{k_{offi}}{\overset{k_{oni}}{\rightleftharpoons}} CaBP_i, \quad i = \text{Cyt, ER or Mt},$$

giving

$$j_{Cai} = k_{offi}[CaBP]_i - k_{oni}[Ca^{2+}]_i([BP]_{Tot_i} - [CaBP]_i), \quad (4)$$

where $[BP]_{Tot_i}$ and $[CaBP]_i$ represent the total concentration of BP and the concentration of Ca^{2+}-bound BP in each compartment, k_{on} and k_{off} denote the on and off rate constants of Ca^{2+} with the BP, respectively.

Ca^{2+} fluxes in ER component. The Ca^{2+} effluxes from the ER to cytosol are given by the IP_3R release and a passive leakage with the concentration gradient across the ER membrane as their driving force, i.e.,

$$j_{ER}^{out} = (v_{IP_3R}P_{oIP_3R} + c_{Leak})([Ca^{2+}]_{ER} - [Ca^{2+}]_{Cyt}), \quad (5)$$

with v_{IP3R} being the maximal efflux from the IP_3Rs in the ER membrane, P_{oIP3R} the open fraction of IP_3Rs, and c_{Leak} the Ca^{2+} leak constant.

The IP_3R channel is an assembly of four equivalent subunits, each of which is mutually gated by IP_3 and Ca^{2+}. The gating dynamics of each IP_3R subunit is described by the Li-Rinzel model[19] and we assumed that the channel is open if at least three of its subunits are in the active state[20]. Thus, we get the following expression for P_{oIP3R}:

$$P_{oIP_3R} = s_{act}^4 + 4s_{act}^3(1\text{-}s_{act}),\ s_{act} = \frac{[IP_3]}{[IP_3] + d_1}\frac{[Ca^{2+}]_{Cyt}}{[Ca^{2+}]_{Cyt} + d_5}h. \quad (6)$$

Here s_{act} is the probability in the active state of the subunit, $[IP_3]$ is the IP_3 concentration, and the slowly gating variable h is given by

$$\frac{dh}{dt} = \alpha_h(1-h) - \beta_h h,\ \alpha_h = a_2 d_2\frac{[IP_3] + d_1}{[IP_3] + d_3},\ \beta_h = a_2[Ca^{2+}]_{Cyt}, \quad (7)$$

where a_i and d_i are constants.

The cytosolic Ca^{2+} can be pumped back into ER by active SERCA which is given by,

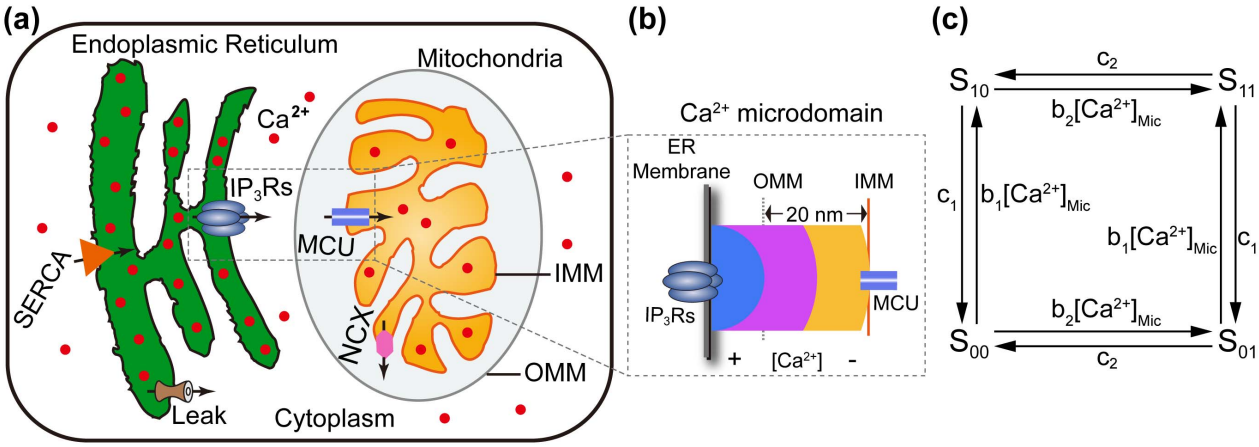

Figure 1 | The model design. (a) The schematic diagram of the components and fluxes included in the model. When a cell is stimulated to generate IP_3, IP_3 binds to IP_3R and triggers Ca^{2+} release from the ER through IP_3Rs. The Ca^{2+} in the cytsol can be pumped back into ER by SERCA. (b) IP_3Rs and MCUs in close proximity form a microdomain, a half 3-dimensional cytosolic space separated by ER membrane. A high microdomain $[Ca^{2+}]$ ($[Ca^{2+}]_{Mic}$) can be generated upon opening of IP_3Rs which in turn leads to Ca^{2+} uptake into mitochondria through MCUs. Ca^{2+} is extruded from mitochondria back into the cytosol by NCX. (c) The four-state model of MCU monomer with binding and unbinding rates.

$$j_{ER}^{in} = \frac{v_{SERCA}[Ca^{2+}]_{Cyt}^2}{k_{SERCA}^2 + [Ca^{2+}]_{Cyt}^2}, \tag{8}$$

where v_{SERCA} and k_{SERCA} are maximum SERCA pump flux and SERCA activation constants.

Ca^{2+} fluxes in mitochondrial component. Mitochondrial Ca^{2+} uptake through MCU is driven primarily by the large voltage across IMM. Besides the IMM voltage, it has been shown that MCU flux is also regulated by MICU[33]. For simplicity, in our model we only consider the role of MICU1 which has been well investigated in experiment. Then the MCU influx can be expressed as

$$j_{Mt}^{in} = v_{MCU}\Delta\Phi R_{MICU} P_{oMCU}. \tag{9}$$

Here v_{MCU} is the maximal flux of MCU, $\Delta\Phi$ is the voltage driving force, R_{MICU} represents the MICU1 regulatory term, and P_{oMCU} describes the open fraction of MCU.

The IMM voltage Ψ is 150 ~ 180 mV (negative inside). Although the net Ca^{2+} flux into the mitochondria might associate with a reduction in voltage, some evidence suggests that mitochondrial Ca^{2+} uptake does not appear to alter Ψ significantly during physiological condition[34]. With the assumption of constant Ψ, the driving force for MCU can be given by[35]

$$\Delta\Phi = \frac{bF(\psi-\psi_0)}{RT} e^{\frac{bF(\psi-\psi_0)}{RT}} \sinh\left(\frac{bF(\psi-\psi_0)}{RT}\right), \tag{10}$$

Here F, R, and T are the Faraday constant, the gas constant and the Kelvin temperature, respectively; b and Ψ_0 are fitting parameters[35].

As a regulatory subunit, MICU1 senses $[Ca^{2+}]$ in mitochondrial intermembrane space to set a threshold for MCU[33]. The influx rate of MCU only becomes substantial when the extra-mitochondrial $[Ca^{2+}]$ reaches values above 3 μM[36]. As a result, the regulation of MICU1 to MCU activity has a sharp activation threshold (k_{MICU}) with an apparent Hill coefficient equal to 4[36]:

$$R_{MICU} = \frac{[Ca^{2+}]_{Mic}^4}{k_{MICU}^4 + [Ca^{2+}]_{Mic}^4}, \tag{11}$$

where $[Ca^{2+}]_{Mic}$ is the microdomain $[Ca^{2+}]_{Cyt}$ that MCU is exposed to, which will be discussed later.

Whereas MICU1 acts as a regulator, MCU represents the core pore-forming component responsible for mitochondrial Ca^{2+} uptake[37,38]. Recent experimental and bioinformatic analysis reveals that MCU is an oligomer[37] and most likely a tetramer[39]. Considering the biphasic dependence of MCU on $[Ca^{2+}]_{Cyt}$, i.e., fast Ca^{2+}-dependent activation and slow Ca^{2+}-dependent inactivation of the MCU[31], we simply propose that each monomer has two Ca^{2+} binding sites, one for activation and another for inhibition. Therefore a monomer can exist in 4 states of s_{00}, s_{10}, s_{01} and s_{11} with the first index for activation binding site and the second index for inhibition binding site and with 1 for binding and 0 unbinding (Fig. 1(c)). Similar as the IP_3R, we posit that the MCU is open if either 3 or 4 of the 4 monomers are in the active state (s_{10}). Thus, the MCU open fraction is given by,

$$P_{oMCU} = (x_{10})^4 + 4(x_{10})^3(1-x_{10}), \tag{12}$$

where x_{ij} denotes the probability of a monomer in states s_{ij}. The dynamical equations governing the state of a monomer are

$$\frac{dx_{00}}{dt} = (c_2x_{01} - b_2[Ca^{2+}]_{Mic}x_{00}) - (b_1[Ca^{2+}]_{Mic}x_{00} - c_1x_{10}),$$

$$\frac{dx_{10}}{dt} = (b_1[Ca^{2+}]_{Mic}x_{00} - c_1x_{10}) - (b_2[Ca^{2+}]_{Mic}x_{10} - c_2x_{11}),$$

$$\frac{dx_{01}}{dt} = (c_1x_{11} - b_1[Ca^{2+}]_{Mic}x_{01}) - (c_2x_{01} - b_2[Ca^{2+}]_{Mic}x_{00}), \tag{13}$$

with $x_{00} + x_{01} + x_{10} + x_{11} = 1$.

Ca^{2+} is extruded from mitochondria primarily by NCX which swaps 3 Na^+ ions with 1 Ca^{2+} ion during each exchange cycle, Thus, the kinetic of outward calcium flux can be described as[35]

$$j_{Mt}^{out} = v_{NCX}\frac{[Na^+]_{Cyt}^3}{k_{Na}^3 + [Na^+]_{Cyt}^3}\frac{[Ca^{2+}]_{Mt}}{k_{NCX} + [Ca^{2+}]_{Mt}}, \tag{14}$$

where $[Na^+]_{Cyt}$ is Na^+ concentration in the cytosol, v_{NCX} is maximal NCX activity, both k_{Na} and k_{NCX} are activation constants for NCX.

Microdomain crosstalk between the ER and mitochondria. Now we describe a microdomain model that represents the crosstalk occurring between closely situated ER and mitochondria

(Fig. 1(b)). The interacting players are IP_3Rs and MCUs in the microdomain. A microdomain of local high $[Ca^{2+}]_{Cyt}$ produced by nearby open IP_3Rs is essential for high capacity Ca^{2+} transport into mitochondria via MCU. It has been reported that 90% of IP_3Rs are located close to mitochondria and the majority of MCU sense the high $[Ca^{2+}]_{Mic}$ in the vicinity of IP_3Rs[29]. Here we make a specific assumption that MCU senses the local high $[Ca^{2+}]_{Mic}$ generated by the opening of clustered IP_3Rs, but other Ca^{2+} handling components, such as IP_3Rs, SERCA, NCX, etc., are determined by the global averaged $[Ca^{2+}]_{Cyt}$. The pros and cons of our method will be discussed in the last section of the paper.

It has been suggested that each mitochondrial Ca^{2+} uptake site must face multiple IP_3Rs for effective mitochondrial Ca^{2+} uptake[40]. Recent experiment evidence indicates that IP_3Rs are typically distributed in clusters on the ER membrane, with each cluster containing a handful of IP_3Rs[41,42]. Patch clamp experiments also show that the Ca^{2+} current (I_{sIP3R}) passing through a single open IP_3R is linearly correlated with the concentration gradient ($[Ca^{2+}]_{ER}$ - $[Ca^{2+}]_{Cyt}$) across the ER membrane with a slope of $S_{IP3R} = 0.3$ pA/mM[43]. Considering the closely distributed IP_3Rs, we treat the Ca^{2+} flux from clustered IP_3Rs as a Ca^{2+} current from a point source at cluster center. As a result, an effective Ca^{2+} current from clustered IP_3Rs is expressed as

$$\delta = n_{IP_3R} P_{oIP_3R} I_{sIP_3R},\ I_{sIP_3R} = S_{IP_3R}([Ca^{2+}]_{ER} - [Ca^{2+}]_{Cyt}). \quad (15)$$

Here, P_{oIP3R} is the IP_3R open probability given by Eq. 6 and n_{IP3R} is the IP_3R number in a cluster. According to Ref. 41, we consider a typical cluster with $n_{IP3R} = 4$. These 4 IP_3Rs are in tight association, organized in a square pattern.

Around the center of IP_3R cluster, the open IP_3Rs will generate a very sharp distribution of $[Ca^{2+}]_{Cyt}$ due to rapid Ca^{2+} diffusion producing a microdomain of high $[Ca^{2+}]_{Cyt}$. Here we also assume that the ER membrane acts as a flat boundary to limit the Ca^{2+} diffusion in a half 3-dimensional space, i.e. the cytosolic microdomian (Fig. 1(b)). Using hemispherical symmetry of Ca^{2+} diffusion from a point release source, the sharp distribution around the release point can be established with a signal equation analogous to the linear cable equation[44,45]. As a solution of the linearized reaction-diffusion equation, the microdomain $[Ca^{2+}]$ is given by[45]

$$[Ca^{2+}]_{Mic} = \frac{\delta}{4\pi r F D_c} e^{(-r/\lambda)} + [Ca^{2+}]_{Cyt}, \quad (16)$$

with

$$\lambda = \sqrt{D_c/(k_{onCyt}[BP]_{Mic} K_d/(K_d + [Ca^{2+}]_{Cyt}))}. \quad (17)$$

Here, D_c is the diffusion coefficient for free Ca^{2+}. The parameter λ is an important factor that determines the sharp decay of $[Ca^{2+}]$ within a microdomain, which accounts for the Ca^{2+} diffusion and binding to BPs. $[BP]_{Mic}$ is the total concentration of BP in the microdomain and K_d is its dissociation constant[44,45]. One can see that the $[Ca^{2+}]_{Mic}$ within a microdomain becomes the cellular average $[Ca^{2+}]_{Cyt}$ when there are no open IP_3Rs.

Eq. 16 describes the $[Ca^{2+}]$ distribution at distance r around the point source, i.e., the IP_3R cluster center. In our model the parameter r is the distance between the MCU and the IP_3R cluster center, which we will call the IP_3R-MCU distance in the paper. Thus, $[Ca^{2+}]_{Mic}$ is the microdomain Ca^{2+} concentration that the MCU sees. Considering MCUs located on IMM, here we also simply assume that the outer mitochondrial membrane (OMM) has little effect on the Ca^{2+} diffusion as it has high permeability to Ca^{2+} [6]. If we suppose the IMM and ER membrane are parallel, parameter r also represents the distance between IMM and ER membrane. As a result, Eq. 16 represents the microdomain coupling between the ER and mitochondria in our model.

Parameter values. The parameters used in this model are listed in Table 1 (see supplementary material). They are categorized on the basis of their source to: (a) those extracted directly from experimental data; (b) those obtained from previously published models; or (c) the free parameters which were fit to experimental results. The model presented in this study permits simultaneous calculation of $[Ca^{2+}]$ changes in the 3 compartments. Currently, it is difficult to measure experimentally Ca^{2+} concentrations in the cytosol and ER or mitochondria simultaneously because of the highly dynamic nature of the Ca^{2+} signals that occur within organelles[46]. Only a few existing experimental data sets[46,47] consist of measurements from all 3 compartments. The free parameters used in our model were extrapolated from fits to these data sets.

Results

The Ca^{2+} oscillations. Our first priority was to determine whether the model realistically simulated cellular Ca^{2+} dynamics. As shown in Fig. 2a, when setting $[IP_3] = 0.5$ μM our model generates baseline Ca^{2+} oscillations occurring as a series of discrete spikes. The values for basal and stimulated $[Ca^{2+}]$ for the cytosol, mitochondria and ER in the model are in close accord with experimental data[38,48]. The oscillations period is in the order of several ten seconds, as seen in many experimental observations with non-exitable cells[2,48]. The Ca^{2+} spikes show relatively rapid rising phases and slow falling phases, mimicking those seen in experimental recordings[49]. The cytosolic and mitochondrial $[Ca^{2+}]$ oscillate almost in phase, with $[Ca^{2+}]_{Cyt}$ as the leader, while the ER $[Ca^{2+}]$ is in anti-phase with them, also as observed experimentally[13,47].

Having established that the salient features of the Ca^{2+} dynamics of our model are in good agreement with existing experimental observations, we examined the effect of manipulating the mechanisms modulated by the crosstalk of the ER and mitochondria. Thus, we also performed simulations in which mitochondria were absent from the model (Fig. 2b). The minimal values of $[Ca^{2+}]_{ER}$ are 311 μM and 276 μM in the absence and in the presence of mitochondria, respectively (Fig. 2), indicating that more Ca^{2+} ions are released from the ER during each spiking cycle in the presence of mitochondria. The maximal values of $[Ca^{2+}]_{Cyt}$ are 5.6 μM and 2.5 μM in the absence and in the presence of mitochondria, respectively (Fig. 2), showing that mitochondria can significantly decrease $[Ca^{2+}]_{Cyt}$ oscillation amplitude.

Ca^{2+} oscillation modulated by IP_3R-MCU distance. Next we looked at the effect of IP_3R-MCU distance on Ca^{2+} oscillation in detail. Fig. 3 compares oscillating $[Ca^{2+}]$ trajectories in microdomain, ER, mitochondria, and cytosol during a single cycle at varying IP_3R-MCU distances. By decreasing the IP_3R-MCU distance from infinity (we used simulations in which mitochondria were absent from the model as the infinite IP_3R-MCU distance), the $[Ca^{2+}]_{Mic}$ in microdomain increases according to Eq. 16 against distance (Fig. 3a), giving an increase in mitochondrial Ca^{2+} uptake. As a result, the minimal $[Ca^{2+}]_{ER}$ steadily decreases (Fig. 3b) and the $[Ca^{2+}]_{Mt}$ spike amplitude steadily increases until saturating at about 65 μM (Fig. 3c). However, an unexpected finding is that the $[Ca^{2+}]_{Cyt}$ spike amplitude first decreases but then increases as the distance decreases (Fig. 3d).

The critical IP_3R-MCU distance. The amplitudes of $[Ca^{2+}]_{Mic}$, $[Ca^{2+}]_{Mt}$, and $[Ca^{2+}]_{Cyt}$ are plotted in detail as a function of distance from 10 to 150 nm at $[IP_3] = 0.5$ μM in Fig. 4a and 4b. A sharp increase is observed for $[Ca^{2+}]_{Mic}$ and $[Ca^{2+}]_{Cyt}$ at $r < 30$ nm, and $[Ca^{2+}]_{Cyt}$ reaches its minimum at $r = 30$ nm. Fig. 4b also shows that the $[Ca^{2+}]_{Cyt}$ spiking period increases monotonically from 30 to

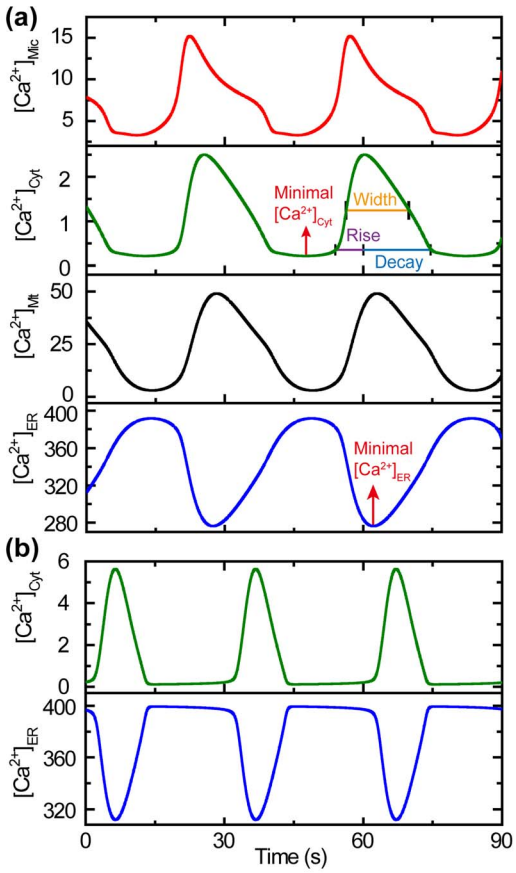

Figure 2 | Mitochondria serve as Ca^{2+} reservoirs. (a) Oscillations of: $[Ca^{2+}]_{Mic}$ in the IP_3R-MCU microdomain, $[Ca^{2+}]_{Cyt}$ in the cytosol, $[Ca^{2+}]_{Mt}$ in mitochondria, and $[Ca^{2+}]_{ER}$ in the ER in the presence of mitochondria with a IP_3R-MCU distance of 35 nm. The width at half maximum, the rising duration and decay duration of $[Ca^{2+}]_{Cyt}$ spike are marked in the second panel of (a). (b) Oscillations of: $[Ca^{2+}]_{Cyt}$ in the cytosol, and $[Ca^{2+}]_{ER}$ in the ER in the absence of mitochondria. $[IP_3] = 0.5$ μM. The unit of $[Ca^{2+}]$ is μM.

50 sec, following the increased ability of mitochondria to take up Ca^{2+} as the IP_3R-MCU distance diminishes. The $[Ca^{2+}]_{Cyt}$ spiking amplitude is determined by the number of Ca^{2+} ions that diffuse into the cytosol, which is related to the total amount of Ca^{2+} ions released from ER through IP_3Rs and the fraction which are taken by mitochondria. In the model, the total amount of Ca^{2+} released from the ER through IP_3R and the fraction accumulated by mitochondria through MCU during each oscillating cycle are plotted in Fig. 4c as a function of IP_3R-MCU distance. The fraction of mitochondrial Ca^{2+} uptake increases monotonically with decreasing distance indicating an increase in the ability of the mitochondria to take up Ca^{2+} at closer distances. Our simulation shows that at 30 nm distance, about 50% of the ER-released Ca^{2+} ions are taken up by mitochondria (see green line with stars in Fig. 4c). As a consequence, $r_{crt} = 30$ nm acts as a critical distance for mitochondria to modulate cytosolic Ca^{2+} signaling: At $r > r_{crt}$, more ER-released Ca^{2+} ions will diffuse into the cytosol than be taken up by mitochondria; whilst at $r < r_{crt}$, mitochondria will capture the majority of Ca^{2+} ions released from ER.

Ca^{2+} dynamics modulated by IP_3R-MCU distance. Surprisingly, Fig. 4c also shows another unexpected finding that the total amount of Ca^{2+} released from the ER first increases with distance down to r = 20 nm and then decreases at smaller distance (see black line with squares in Fig. 4c). This raises a critical question: with decreasing distance at $r < 20$ nm, how can $[Ca^{2+}]_{Cyt}$ spiking amplitudes increase (violet line with diamonds in Fig. 4b), while the total amount of Ca^{2+} released from the ER decreases (black line with squares in Fig. 4c) but mitochondrial Ca^{2+} uptake fraction increases (green line with stars in Fig. 4c)?

In order to further examine this conflicting effect of distance on $[Ca^{2+}]_{Cyt}$ spike amplitude and the amount of ER-released Ca^{2+}, we investigated how mitochondrial Ca^{2+} uptake modulates the spike width, the spike rising time and decay time of $[Ca^{2+}]_{Cyt}$ at varying IP_3R-MCU distance. Here the spike width is defined as the duration at half maximum of $[Ca^{2+}]_{Cyt}$ spike amplitude, the rising time is defined as the duration from twice of the minimal $[Ca^{2+}]_{Cyt}$ to the peak of the response, and the decay time as the duration from the peak of the response to twice of the minimal $[Ca^{2+}]_{Cyt}$. An example of definition of these parameters is marked in Fig. 2a for spike curve at distance r = 35 nm.

We first discuss the simple situation at $r > r_{crt}$. As shown in Fig. 4d when $r > r_{crt}$, the spike width increases with decreasing distance, which primarily arises from an increase in the duration of the decay time, whereas the rising time is rapid and shows little change with distance. As r decreases, the ability of mitochondrial Ca^{2+} uptake increases, leading to a decrease in $[Ca^{2+}]_{Cyt}$ amplitude. The decrease in $[Ca^{2+}]_{Cyt}$ amplitude in turn leads to a weakening of the Ca^{2+} inhibition of IP_3R dynamics, resulting in the prolonged spike decay time with decreasing distance.

Differently, at $r < r_{crt}$, as the IP_3R-MCU distance decreases, even though the rising time increases (black line in Fig. 4d), the spike width actually becomes smaller due to a decrease in the decay time (blue and red lines in Fig. 4d). At this small distance, the rising time consists of both a slow rising phase and an abrupt rising phase. As an example, the slow rising and abrupt rising phases for a spike at distance r = 10 nm are indicated by arrows in Fig. 3a&b. The mitochondrial Ca^{2+} uptake is so strong that, at the beginning of each oscillating cycle, most of the ER-released Ca^{2+} ions are directly driven into mitochondria, leading to a rapid increase of $[Ca^{2+}]_{Mt}$ (Fig. 3c), but a very slow increase of $[Ca^{2+}]_{Cyt}$ (Fig. 3d). With low $[Ca^{2+}]_{Cyt}$, there are a small fraction of activating IP_3Rs which remain open for a long time, resulting in a slow rise phase for $[Ca^{2+}]_{Cyt}$ (e.g. the gray dash line for r = 10 nm in Fig. 3d with time from 0 to 30 sec). Such a long duration with low $[Ca^{2+}]_{Cyt}$ actually contributes little to the spike width. When $[Ca^{2+}]_{Mt}$ increases to approach to its saturation state, most of the ER-released Ca^{2+} ions will then diffuse into cytosol. Because of the Ca^{2+} induced Ca^{2+} release, there occurs an abrupt increase in the numbers of open IP_3Rs, generating a spike (e.g. the gray dash line for r = 10 nm in Fig. 3d with time from 30 to 35 sec).

With shorter IP_3R-MCU distance, the mitochondria become more saturated prior to the abrupt rising phase, and thus during the abrupt rising phase the Ca^{2+} ions released from the ER diffuse more into cytosol, generating a higher amplitude spike in $[Ca^{2+}]_{Cyt}$ (violet line with diamonds in Fig. 4b at $r < 30$ nm). In turn, the elevated $[Ca^{2+}]_{Cyt}$ peak induces a strong inhibitory effect on IP_3R dynamics, such that spikes decay faster as the IP_3R-MCU distance decreases (red line with circles in Fig. 4d).

The changes with distance seen in the amount of Ca^{2+} ions released from the ER during the rise and decay phases can then explain why the total amount of ER-released Ca^{2+} reaches a maximum around r = 20 nm. At $r > r_{crt}$, as the rising time is fast and little affected by distance (close to 6 s as shown in Fig. 4d), the elevation in the total amount of ER-released Ca^{2+} with decreasing distance mainly related to the increase of the decay phase. By decreasing r at $r_{crt} > r > 20$ nm, although the amount of ER-released Ca^{2+} ions during the decay phase decreases because of the shortened decay duration (red line in Fig. 4d), the amount of ER-released Ca^{2+} ions during the rising phase increases because of the prolonged rising duration (black line in Fig. 4d). As a result, the total amount of Ca^{2+}

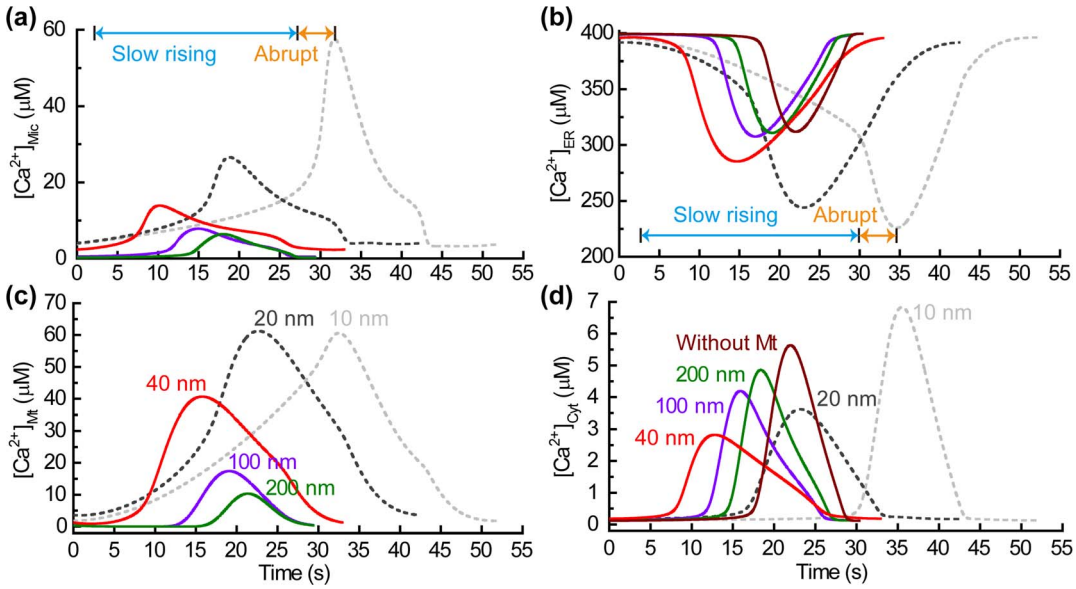

Figure 3 | The time evolution of $[Ca^{2+}]_{Mic}$ (a), $[Ca^{2+}]_{ER}$ (b), $[Ca^{2+}]_{Mt}$ (c) and $[Ca^{2+}]_{Cyt}$ (d) in an oscillating cycle at distance r = 200 (green), 100 (purple), 40 (red), 20 (dark) and 10 nm (grey). The brown lines in (b) and (d) are in the absence of mitochondria. In (a) and (b) the duration of an abrupt increase in Ca^{2+} release is marked by arrows for r = 10 nm. $[IP_3]$ = 0.5 μM.

released by ER keeps increasing with decreasing r for $r_{crt} > r >$ 20 nm. However, at very short distance of r < 20 nm, during the rising phase the ER-released Ca^{2+} ions almost saturate both mitochondria and the cytosol, giving a maximal Ca^{2+} amount released by ER during the rising phase (see the open circles in Fig. 4c at r < 20 nm). Then, the change of the total amount of ER-released Ca^{2+} is typically determined by the change of decay time, leading to a decrease in the total amount of ER-released Ca^{2+} with decreasing distance at r < 20 nm.

Thus we can see how the apparently paradoxical relationship between $[Ca^{2+}]_{Cyt}$ spike amplitude and total amount of ER-released Ca^{2+} at IP_3R-MCU distances <20 nm develops. At r < 20 nm, the $[Ca^{2+}]_{Cyt}$ spike amplitude is mainly determined by the amount of Ca^{2+} released during the abrupt rising phase of a Ca^{2+} response, giving an increasing relationship with decreasing distance. In contrast to this, the change in the total amount of ER-released Ca^{2+} mainly follows the behavior of the spike decay time, giving a decreasing relationship with decreasing distance at r < 20 nm.

The synchronization of the oscillation phases between $[Ca^{2+}]_{Cyt}$, $[Ca^{2+}]_{ER}$, and $[Ca^{2+}]_{Mt}$ is also modulated by the IP_3R-MCU distance. Our data (not shown here) indicate that at $r > r_{crt}$, $[Ca^{2+}]_{Cyt}$ peaks first, followed by $[Ca^{2+}]_{ER}$ minimum and then $[Ca^{2+}]_{Mt}$ peak, due to an increase of the amount of ER-released Ca^{2+} ions diffusing into the cytosol at greater distances. However, when $r < r_{crt}$, more ER-

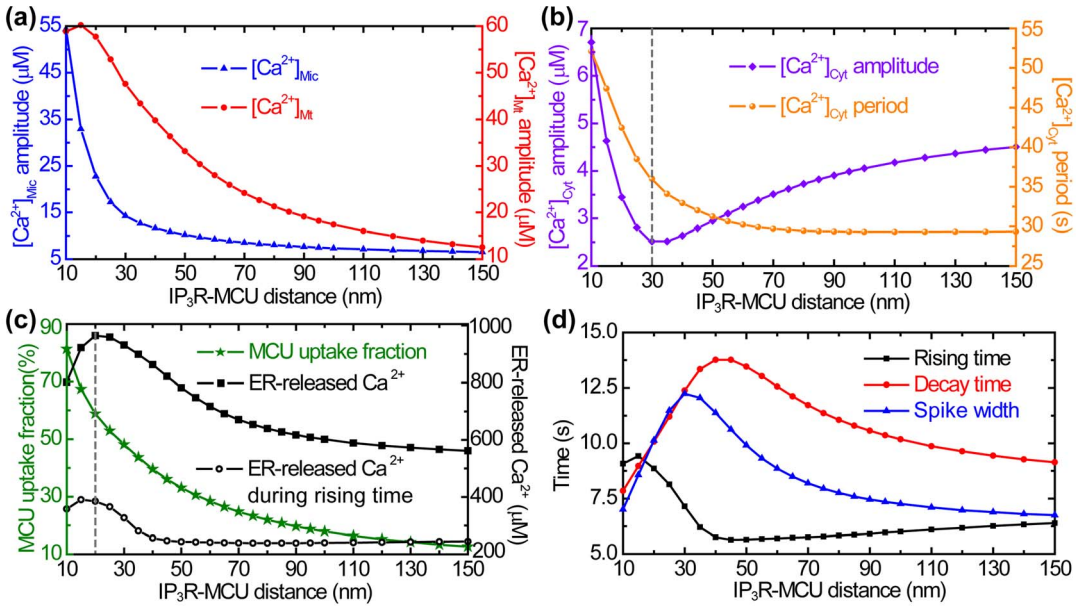

Figure 4 | **Ca^{2+} dynamics modulated by the IP_3R-MCU distance.** (a) The spike amplitudes of $[Ca^{2+}]_{Mic}$ (triangles) and $[Ca^{2+}]_{Mt}$ (circles). (b) The spike amplitudes of $[Ca^{2+}]_{Cyt}$ (diamonds) and spike period (spheres). (c) The total amount of Ca^{2+} released from the ER through IP_3Rs during each cycle (squares), the amount of Ca^{2+} released from the ER through IP_3Rs during the rising time (circles), and the fraction delivered to mitochondria through MCU (stars). (d) The spike width (triangles), the rising time (squares) and the decay time (circles) of $[Ca^{2+}]_{Cyt}$ oscillations. $[IP_3]$ = 0.5 μM.

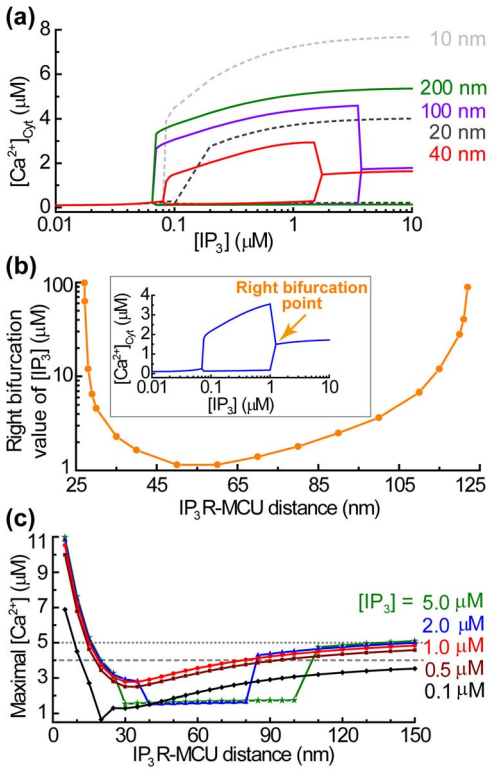

Figure 5 | Ca^{2+} dynamics modulated by $[IP_3]$. (a) The bifurcation diagram (the stable steady states and the maxima and minima of Ca^{2+} oscillations) of the model with $[IP_3]$ as the bifurcation parameter at distance r = 200 (green), 100 (purple), 40 (red), 20 (dark) and 10 nm (grey). (b) The value of $[IP_3]$ at the right bifurcation point plotted against distance. The inset is the bifurcation diagram at distance r = 60 nm, in which the arrow marks the right bifurcation point. (c) The maximal $[Ca^{2+}]_{Cyt}$ against the IP_3R-MCU distance for $[IP_3]$ = 0.1 (lozenges), 0.5 (squares), 1.0 (circles), 2.0 (triangles), and 5.0 μM (stars). The dashed and dotted lines represent $[Ca^{2+}]_{Cyt}$ = 4 and 5 μM, respectively.

released Ca^{2+} ions are sequestered into mitochondria, so $[Ca^{2+}]_{Mt}$ peaks first, followed by $[Ca^{2+}]_{ER}$ minimum and then $[Ca^{2+}]_{Cyt}$ peak.

Ca^{2+} dynamics modulated by $[IP_3]$. In the following discussion, we investigate how $[IP_3]$ controlled $[Ca^{2+}]_{Cyt}$ oscillations can be modulated by the IP_3R-MCU distance. The bifurcation diagram for $[Ca^{2+}]_{Cyt}$ oscillation (i.e. the steady state of $[Ca^{2+}]_{Cyt}$ or the maximum and minimum of $[Ca^{2+}]_{Cyt}$ oscillation) with $[IP_3]$ as the bifurcation parameter is plotted at different IP_3R-MCU distances in Fig. 5a. When IP_3 levels are low, $[Ca^{2+}]_{Cyt}$ can be seen to remain in a low stable steady state. Beyond a certain threshold value of $[IP_3]$, $[Ca^{2+}]_{Cyt}$ undergoes periodical oscillations. We also found that, at distance range of 27–122 nm, the system only demonstrates sustained Ca^{2+} oscillations when $[IP_3]$ values are in an intermediate range, evolving into a stable steady state at higher $[IP_3]$ (Fig. 5b). Such a bifurcation diagram for r = 60 nm is depicted in the inset of Fig. 5b. Similar bifurcation behavior has been observed in the experimental Ca^{2+} waves in *Xenopus laevis* oocytes. In oocytes it has been shown that repetitive Ca^{2+} waves occur only at intermediate $[IP_3]$ between 0.1 and 1 μM[50]. Thus, as shown in the inset of Fig. 5b, r = 60 nm is the optimum IP_3R-MCU distance in which our model replicates these experimental observations. According to the experiment[50], for a biologically meaningful Ca^{2+} oscillation model there should be a right bifurcation point for high $[IP_3]$, beyond which there occurs no Ca^{2+} oscillation. As plotted in Fig. 5b, only in the range of r of 27–122 nm the model can produce Ca^{2+} oscillations in an intermediate $[IP_3]$ range. Outside of such distance range the Ca^{2+} oscillations always occur even at infinitely high $[IP_3]$ (Fig. 5b).

$[Ca^{2+}]_{Cyt}$ oscillations with limited amplitudes regulate a host of vital cell functions[1]. A global $[Ca^{2+}]_{Cyt}$ less than 3.5 μM is usually observed in living cell[38,48]. However, high $[Ca^{2+}]_{Cyt}$ will trigger and modulate apoptosis[51]. Fig. 5c shows the maximal $[Ca^{2+}]_{Cyt}$ values seen in our model plotted against IP_3R-MCU distance for different $[IP_3]$. One can see that a rapid elevation in $[Ca^{2+}]_{Cyt}$ amplitude is observed at IP_3R-MCU distances around 10 nm. A global $[Ca^{2+}]_{Cyt}$ which is smaller than 4.0 or 5.0 μM (i.e. dashed or dotted line in Fig. 5c) is typically obtained with IP_3R-MCU distances of 20 to 85 nm or distances of 15 to 150 nm, respectively.

Robustness with varying clustered IP_3R number. In above study, we only consider a cluster in which n_{IP3R} = 4 IP_3Rs correspond to a single MCU. Experimental evidence suggests that IP_3R clusters typically contain a handful (~4) of IP_3Rs[41,42]. Next we discuss the robustness of the model's behavior upon slight changes in n_{IP3R} (from 4 to 3, and 5). By calculating the fraction of Ca^{2+} ions accumulated by mitochondria compared to the total amount of Ca^{2+} released from the ER, we see that the critical distance is changed to 20 nm for n_{IP3R} = 3 and 35 nm for n_{IP3R} = 5 (Fig. 6(a)). Fig. 6(b) gives the value of $[IP_3]$ at the right bifurcation point against distance with varying n_{IP3R}. A common region to find the right bifurcation $[IP_3]$ is obtained with distances of 33 to 93 nm. Fig. 6(c) shows the maximal $[Ca^{2+}]_{Cyt}$ plotted against IP_3R-MCU distances for varying n_{IP3R}. A global $[Ca^{2+}]_{Cyt}$ which is smaller than 4.0 or 5.0 μM (i.e. dashed or dotted line in Fig. 6(c)) is

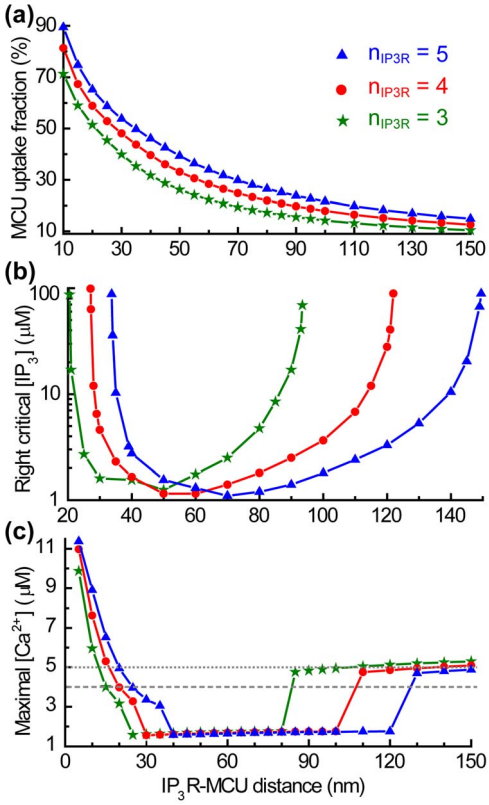

Figure 6 | Robustness of Ca^{2+} dynamics on n_{IP3R}. (a) The fraction of Ca^{2+} accumulated by mitochondria of the total amount of Ca^{2+} released from the ER during each oscillating cycle plotted against IP_3R-MCU distance. (b) The value of $[IP_3]$ at the right bifurcation point against distance. (c) The maximal $[Ca^{2+}]_{Cyt}$ against the IP_3R-MCU distance at saturating $[IP_3]$ = 5.0 μM. The dashed and dotted lines represent $[Ca^{2+}]_{Cyt}$ = 4 and 5 μM, respectively. Here n_{IP3R} = 3 (stars), 4 (circles) and 5 (triangles).

typically obtained with IP_3R-MCU distances of 25 to 85 nm or distances of 20 to 110 nm, respectively.

Taken together, compared with experimental observations[38,48,50,51], the simulation results shown in Fig. 5 and Fig. 6 suggest that the optimal IP_3R-MCU distance for physiological Ca^{2+} signaling should be around 30 to 85 nm. When the IP_3R-MCU distance is between 30 and 85 nm, as illustrated in Fig. 6(a) approximately 15–55% of ER-released Ca^{2+} ions can be taken up by mitochondria, compatible with experimental measurements made in various cells[52,53]. Our model thus suggests that mitochondria, typically working at a short distance from the ER (but larger than r_{crt}), serve as Ca^{2+} sinks, sequestering Ca^{2+} ions released from the ER.

Discussion

Since the 1990s, the manner in which mitochondrial Ca^{2+} uptake through MCU shapes intracellular Ca^{2+} signaling has attracted much attention[6]. The key questions presently debated are: to what extent mitochondria acquire Ca^{2+}; what impact mitochondria have on cytosolic Ca^{2+} signals; and what dimensions the ER/mitochondria Ca^{2+} microdomain might have. To address these questions, we constructed a Ca^{2+} signaling model to consider the Ca^{2+} crosstalk within microdomains between IP_3Rs and MCU. A 4-states MCU model has been suggested based on the latest experimental results[31,37–39]. The MCU is exposed to the microdomain Ca^{2+} concentration which is released from the nearby clustered IP_3Rs[34,36], rather than the bulk cytosolic Ca^{2+} concentration. As a result, the model replicates the shape, amplitude, period, and kinetics of the Ca^{2+} spikes observed in experimental data, allowing us to examine the effects of mitochondrial Ca^{2+} uptake on cytosolic Ca^{2+} signals.

From experimental observations, it has been suggested that mitochondrial Ca^{2+} uptake contributes significantly to the physiological regulation of cytosolic Ca^{2+}[38]. Regarding the recent controversy whether mitochondria act as significant buffers to cytosolic Ca^{2+} under physiological conditions[17], our model indicates that mitochondria can accumulate large quantities of Ca^{2+} under physiological conditions (about 15–55% of the total released from the ER) at IP_3R-MCU distances of 30–85 nm. Furthermore, our model indicates that the distance between the ER and mitochondria appears to be an important factor in modulating Ca^{2+} signaling, especially considering that mitochondria can be highly mobile organelles[54]. There is a critical IP_3R-MCU distance r_{crt} (around 20 to 35 nm depending on n_{IP3R}) at which half of the Ca^{2+} released by the ER is taken up by mitochondria. At distances smaller than r_{crt} mitochondria can take up more Ca^{2+}, while at distances larger than r_{crt}, more Ca^{2+} ions diffuse from the ER into the cytosol. This leads to mitochondria displaying different kinds of Ca^{2+} signal modulation depending on their distance from the ER. The effects of mitochondria on the spike amplitude, spike width, and rising and decay time of $[Ca^{2+}]_{Cyt}$ spikes, the synchronization phase among $[Ca^{2+}]_{Cyt}$, $[Ca^{2+}]_{ER}$ and $[Ca^{2+}]_{Mt}$, and the total amount of Ca^{2+} released from the ER are all substantially modulated by how the IP_3R-MCU distance deviates from this critical value.

To explore experimentally the consequences of mitochondrial Ca^{2+} uptake on global Ca^{2+} signals, mitochondrial Ca^{2+} uptake is often prevented directly by applying an MCU inhibitor[14] or modulated by using agents which either depolarize or hyperpolarize the mitochondrial membrane potential and thus dissipate or increase the driving force for Ca^{2+} uptake into the organelle[10,14]. How mitochondrial Ca^{2+} uptake affects IP_3R release mechanism is still under investigation. Some researchers have argued that mitochondrial Ca^{2+} uptake may provide a positive modulation of Ca^{2+} release by suppressing the negative feedback of high $[Ca^{2+}]_{Cyt}$ on IP_3R[9–11]. Others have suggested that mitochondrial Ca^{2+} uptake exerts a negative control on $[Ca^{2+}]_{Cyt}$ by preventing the positive feedback of Ca^{2+} on IP_3R[12,13].

In our simulations, the ability of mitochondria to take up Ca^{2+} is changed by varying the IP_3R-MCU distance and so the mitochondrial modulation on IP_3R dynamics has been examined. Our model indicates that altering mitochondrial Ca^{2+} uptake induces a nontrivial change on $[Ca^{2+}]_{Cyt}$ amplitude, which can reconcile the conflicting results of the change of $[Ca^{2+}]_{Cyt}$ amplitude observed in various experiments[9–13]. When IP_3R-MCU distance is larger than the critical distance r_{crt}, mitochondrial Ca^{2+} uptake is weak and more Ca^{2+} ions diffuse into cytosol, the enhancement of mitochondrial Ca^{2+} uptake causes a decreasing $[Ca^{2+}]_{Cyt}$ spike peak, exerting a weakened inhibition effect on IP_3R dynamics, resulting in a prolonged decay time of spikes. Thus, at this region, mitochondrial Ca^{2+} uptake offers a positive modulation of Ca^{2+} release by reducing $[Ca^{2+}]_{Cyt}$ amplitude to suppress the inhibition dynamics (i.e. the negative feedback) of high $[Ca^{2+}]_{Cyt}$ on IP_3R during decay time of spikes (Fig. 7), similar as suggested in refs 9, 10, 11. While, when IP_3R-MCU distance is smaller than the critical distance, mitochondria take more Ca^{2+} ions than those diffusing into cytosol, the strong mitochondrial Ca^{2+} uptake will force $[Ca^{2+}]_{Cyt}$ at a small value to prevent the strong activation

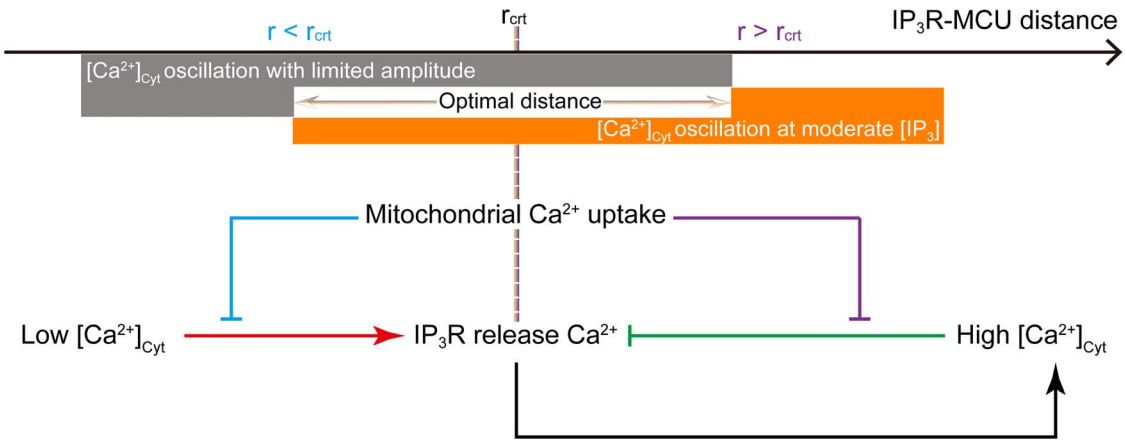

Figure 7 | Schematic representation of how mitochondria modulate $[Ca^{2+}]_{Cyt}$. IP_3R channel is regulated by Ca^{2+} in a biphasic manner: a lower $[Ca^{2+}]_{Cyt}$ promotes Ca^{2+} release and causes its elevation whereas higher $[Ca^{2+}]_{Cyt}$ inhibits Ca^{2+} release. There is a critical distance at which 50% of the IP_3R-released Ca^{2+} ions are taken up by mitochondria. When $r<r_{crt}$, mitochondrial Ca^{2+} uptake exerts a negative control on IP_3R-released Ca^{2+} by preventing the positive effect of low $[Ca^{2+}]_{Cyt}$ on IP_3R; whilst when $r > r_{crt}$, mitochondrial Ca^{2+} uptake provides a positive modulation on IP_3R-released Ca^{2+} by suppressing the negative effect of high $[Ca^{2+}]_{Cyt}$ on IP_3R. Ca^{2+} oscillations merely occur for moderate values of $[IP_3]$ (orange range) with physiological amplitude (gray range), so the optimal distance of IP_3R-MCU should be within the intersection zone between the gray and orange range.

dynamics (i.e. the positive feedback) of $[Ca^{2+}]_{Cyt}$ on IP_3R (Fig. 7), similar as proposed in refs 12, 13. Thus, our model shows that this weak activation effect causes a small Ca^{2+} release from ER, giving a slow rising phase. When mitochondria approach to saturation and $[Ca^{2+}]_{Cyt}$ increases beyond the threshold of excitable dynamics, an abrupt rising phase occurs to generate a $[Ca^{2+}]_{Cyt}$ spike, giving a high $[Ca^{2+}]_{Cyt}$ amplitude and then inducing a strong inhibitory effect on IP_3R dynamics to shorten the decay time of spikes.

An unexpected prediction with the model is that when the IP_3R-MCU distance is less than the critical distance, even though mitochondrial Ca^{2+} uptake keeps increasing with decreasing distance, the total amount of Ca^{2+} released from the ER decreases while the cytosolic Ca^{2+} spike amplitude increases. The $[Ca^{2+}]_{Cyt}$ peak is mainly determined by the amount of Ca^{2+} released during the abrupt rising phase of spikes. At shorter IP_3R-MCU distances, the mitochondria become almost saturated before the abrupt rising phase, and thus during the abrupt rising phase more of the Ca^{2+} ions released from the ER diffuse more into cytosol, generating a higher amplitude of $[Ca^{2+}]_{Cyt}$. However, the change in the total amount of Ca^{2+} release from the ER seen with decreasing distance is mainly determined by the release of Ca^{2+} occurring during the decay phase of spike. The enhanced inhibitory effect of higher amplitude $[Ca^{2+}]_{Cyt}$ spikes on IP_3R dynamics in turn leads to a shortening of the decay time of the spikes, resulting in a decrease in the total Ca^{2+} amount released from ER with decreased IP_3R-MCU distance.

The existence of high $[Ca^{2+}]_{Mic}$ in microdomains has been put forward as one way to resolve the apparent paradox that even though the Ca^{2+} affinity of the MCU is low (K_d of 10–20 μM) highly efficient mitochondrial Ca^{2+} uptake still occurs under physiological conditions with low micromolar global $[Ca^{2+}]_{Cyt}$[3]. However, an intriguing question related to the role of the microdomain is the distance between the ER and mitochondria that would be required to control distinct cellular processes. The distance from the ER membrane to OMM was originally estimated to be in excess of 100 nm[16], recently it has been suggested that this distance could be in the order of 30 nm[15,55]. A key prediction of our model is that the optimal distance between the IP_3R and MCU is about 30–85 nm. This arises when parameters for $[IP_3]$ and $[Ca^{2+}]$ are derived from the experimental observations that Ca^{2+} oscillations generally occur for intermediate values of IP_3[50] and that physiological $[Ca^{2+}]_{Cyt}$ amplitudes seldom exceed 3.5 μM in living cells[38,48], which are illustrated in Fig. 7. Considering that the thickness between OMM and IMM is around 20 nm[56], our model predicts that the optimal gap between the ER membrane and OMM should be approximately 10–65 nm, which is in good agreement with measurements obtained via electron microscopy and tomography[15,31,55].

Interestingly, our simulation also provides a reason for why MCUs need to be located ~20 nm away from the OMM. In experiment, elevations in the magnitude of $[Ca^{2+}]_{Cyt}$ during typical agonist induced responses could lead to a triggering of $[Ca^{2+}]_{Cyt}$-induced apoptosis[51]. Maintaining a distance between IMM and OMM of 20 nm may present a defense mechanism to keep the global $[Ca^{2+}]_{Cyt}$ at a small physiological range. Our model highlights the importance of the IP_3R-MCU distance and suggests that potential pathological mechanisms for generating elevated $[Ca^{2+}]_{Cyt}$ and leading to possibly $[Ca^{2+}]_{Cyt}$-induced apoptosis[6,51] would be found in disorders in which the optimal distance between the ER and mitochondria is disturbed. Considering that when untethered to the ER, mitochondria can be highly mobile organelles[54] and that little is known of the physiological stimuli governing the distance between the ER and mitochondria, or how the tethers between the ER and mitochondria function or are disrupted during pathology, future research elucidating how the IP_3R-MCU distance is maintained and controlled is essential.

Finally, we discuss the advantages and limitations of our model. First, the previous published models typically simulated MCU either by a simple Hill equation[26,29] or by the Monod-Wyman-Changeux type allosteric regulation[24,27,28]. In contrast to these models, we introduced a mechanistic kinetic model to discuss in detail the binding and unbinding processes of Ca^{2+} to MCU. Second, the numerical simulation about the peak values of $[Ca^{2+}]_{ER}$ or/and $[Ca^{2+}]_{Mt}$ were usually underestimated in most of the models[24,26–30]. For example, the concentration of free Ca^{2+} in the ER is typically in the range of a few hundred micromolars. Our model is capable of reproducing the observed magnitudes of $[Ca^{2+}]_{Cyt}$, $[Ca^{2+}]_{ER}$ and $[Ca^{2+}]_{Mt}$.

In 2013, Szopa et al. suggested a model to explicitly take into account the existence of Ca^{2+} microdomain between the ER and mitochondria to discuss the mitochondrial Ca^{2+} uptake[29]. However, the assumption in the model that MCU directly senses the $[Ca^{2+}]_{ER}$ may be not very appropriate, particularly in view of the existing sharp Ca^{2+} gradients in the microdomain against the distance between the IP_3R and MCU. Previously, there are mainly two basic ways to handle Ca^{2+} microdomain in the whole-cell models. The first approach involved the separation of a specified small region from the cell. But this subspace is simply treated as another well-mixed compartment[57,58], and thus this approach cannot capture the fact of sharp Ca^{2+} concentration gradients in the microdomain[43,44]. Sneyd et al. used an alternative approach to divide the cell into a few separate domains, connected by many boundary fluxes[59,60]. Although this is a powerful approach, it greatly increases the complexity of the model, leading to extreme computational difficulties.

Different from these methods, a new approach has been suggested in the present paper. For simplicity, all the IP_3Rs dynamics and SERCA are determined by the bulk $[Ca^{2+}]_{Cyt}$. As a result, the bulk Ca^{2+} concentrations in cytosol, ER and mitochondria can be examined in deterministic ODE which actually assuming that the cytosolic, ER and mitochondrial compartments are mixed homogenously. Upon such well mixed compartments, a microdomain is specifically considered to discuss the MCU dynamics which is crucial for mitochondrial Ca^{2+} uptake. The microdomain consists of a cluster of IP_3Rs and a MCU separated at a short distance. Treated as a point release source for the clustered IP_3Rs which dynamics is controlled by bulk $[Ca^{2+}]_{Cyt}$, a sharp distribution of $[Ca^{2+}]_{Mic}$ can be built up in the microdomain. Each MCU responds to the local high $[Ca^{2+}]_{Mic}$ generated by the clustered IP_3Rs, rather than the bulk $[Ca^{2+}]_{Cyt}$. As a result, this method avoids the simulation of the Ca^{2+} diffusion in microdomain between the ER membrane and IMM.

Peglow et al.[30] discussed a three-dimensional model to analyze the influence of the distance between mitochondria and the CRAC channel on the plasma membrane, which is responsible for Ca^{2+} influx from the outside of the cell, on global Ca^{2+} oscillation. They confirmed that the relative position between mitochondria and the CRAC channels controls the global Ca^{2+} signal. Their simulation results showed that close mitochondria will lower the microdomain $[Ca^{2+}]$ right at the CRAC channels and prevent the Ca^{2+}-dependent inactivation of CRAC channels, leading to higher Ca^{2+} influx and thereby increasing global $[Ca^{2+}]_{Cyt}$. They found that the global $[Ca^{2+}]_{Cyt}$ monotonously changes with the mitochondria-CRAC distance from 0.1 to 2 μm. A similar result is obtained in our model at $r > r_{crt}$.

As a fact, our model does not realistically consider the spatial structure and so many important factors of Ca^{2+} signaling have been ignored. In the model the microdomain is modeled as a radially symmetric hemisphere and so the linearized reaction-diffusion equation has been applied to obtain a simple expression for $[Ca^{2+}]_{Mic}$. The mitochondrial boundary is actually ignored. One may expect that the mitochondrial boundary effect may modulate the sharp $[Ca^{2+}]_{Mic}$ distribution. The Ca^{2+} release from the clustered IP_3Rs are treated as the point release source, which is correct for far away MCU. But if MCU is too close to IP_3Rs, a better treatment is to consider the spatial distribution of IP_3Rs. The model also assumes that OMM has no effect on the Ca^{2+} diffusion as it has high permeability to Ca^{2+}. A

better MCU model should also consider the regulation effect of MICU2 on the MCU channel activity. Our model is primarily designed for non-excitable cells, i.e. a 'closed' cell model, ignoring the Ca^{2+} exchange between cytosol and extracellular medium through the plasma membrane. Thus, a more realistic Ca^{2+} model should be considered in the future. However, despite oversimplification in some details, we believe that the present model is useful and may provide us some insights on how the crosstalk between the ER and mitochondria modulates Ca^{2+} signals in living cells.

1. Berridge, M. J., Bootman, M. D. & Roderick, H. L. Calcium signalling: dynamics, homeostasis and remodelling. *Nat. Rev. Mol. Cell Bio.* **4**, 517–529 (2003).
2. Parekh, A. B. Decoding cytosolic Ca^{2+} oscillations. *Trends Biochem. Sci.* **36**, 78–87 (2011).
3. Contreras, L., Drago, I., Zampese, E. & Pozzan, T. Mitochondria: the calcium connection. *BBA-Bioenergetics* **1797**, 607–618 (2010).
4. Rizzuto, R., Brini, M., Murgia, M. & Pozzan, T. Microdomains with high Ca^{2+} close to IP_3-sensitive channels that are sensed by neighboring mitochondria. *Science* **262**, 744–747 (1993).
5. Hajnóczky, G., Robb-Gaspers, L. D., Seitz, M. B. & Thomas, A. P. Decoding of cytosolic calcium oscillations in the mitochondria. *Cell* **82**, 415–424 (1995).
6. Rizzuto, R., De Stefani, D., Raffaello, A. & Mammucari, C. Mitochondria as sensors and regulators of calcium signalling. *Nat. Rev. Mol. Cell Bio.* **13**, 566–578 (2012).
7. Giacomello, M. *et al.* Ca^{2+} Hot Spots on the Mitochondrial Surface Are Generated by Ca^{2+} Mobilization from Stores, but Not by Activation of Store-Operated Ca^{2+} Channels. *Mol. Cell* **38**, 280–290 (2010).
8. Csordás, G. *et al.* Imaging interorganelle contacts and local calcium dynamics at the ER-mitochondrial interface. *Mol. Cell* **39**, 121–132 (2010).
9. Jouaville, L. S., Ichas, F., Holmuhamedov, E. L., Camacho, P. & Lechleiter, J. D. Synchronization of calcium waves by mitochondrial substrates in *Xenopus laevis* oocytes. *Nature* **377**, 438–441 (1995).
10. Vay, L. *et al.* Modulation of Ca^{2+} release and Ca^{2+} oscillations in HeLa cells and fibroblasts by mitochondrial Ca^{2+} uniporter stimulation. *J. Physiol.* **580**, 39–49 (2007).
11. Olson, M. L., Chalmers, S. & McCarron, J. G. Mitochondrial Ca^{2+} uptake increases Ca^{2+} release from inositol 1, 4, 5-trisphosphate receptor clusters in smooth muscle cells. *J. Biol. Chem.* **285**, 2040–2050 (2010).
12. Boitier, E., Rea, R. & Duchen, M. R. Mitochondria exert a negative feedback on the propagation of intracellular Ca^{2+} waves in rat cortical astrocytes. *J. Cell Biol.* **145**, 795–808 (1999).
13. Hajnóczky, G., Hager, R. & Thomas, A. P. Mitochondria suppress local feedback activation of inositol 1, 4, 5-trisphosphate receptors by Ca^{2+}. *J. Biol. Chem.* **274**, 14157–14162 (1999).
14. Olson, M. L., Chalmers, S. & McCarron, J. G. Mitochondrial organization and Ca^{2+} uptake. *Biochem. Soc. Trans.* **40**, 158–167 (2012).
15. Csordás, G. *et al.* Structural and functional features and significance of the physical linkage between ER and mitochondria. *J. Cell Biol.* **174**, 915–921 (2006).
16. de Brito, O. M. & Scorrano, L. An intimate liaison: spatial organization of the endoplasmic reticulum–mitochondria relationship. *EMBO J.* **29**, 2715–2723 (2010).
17. Williams, G. S., Boyman, L., Chikando, A. C., Khairallah, R. J. & Lederer, W. Mitochondrial calcium uptake. *Proceedings of the National Academy of Sciences* **110**, 10479–10486 (2013).
18. Meyer, T. & Stryer, L. Molecular model for receptor-stimulated calcium spiking. *Proc. Nat. Acad. Sci.USA* **85**, 5051–5055 (1988).
19. Li, Y. X. & Rinzel, J. Equations for $InsP_3$ Receptor-mediated $[Ca^{2+}]_i$ Oscillations Derived from a Detailed Kinetic Model: A Hodgkin-Huxley Like Formalism. *J. Theor. Biol.* **166**, 461–473 (1994).
20. Shuai, J. W. & Jung, P. Stochastic Properties of Ca^{2+} Release of Inositol 1, 4, 5-Trisphosphate Receptor Clusters. *Biophys. J.* **83**, 87–97 (2002).
21. Shuai, J. W. & Jung, P. Optimal ion channel clustering for intracellular calcium signaling. *Proc. Nat. Acad. Sci.USA* **100**, 506–510 (2003).
22. Rüdiger, S., Shuai, J. W. & Sokolov, I. Law of mass action, detailed balance, and the modeling of calcium puffs. *Phys. Rev. Lett.* **105**, 048103 (2010).
23. Rüdiger, S. Stochastic models of intracellular calcium signals. *Phys. Rep.* **534**, 39–87 (2014).
24. Cortassa, S., Aon, M. A., Marbán, E., Winslow, R. L. & O'Rourke, B. An integrated model of cardiac mitochondrial energy metabolism and calcium dynamics. *Biophys. J.* **84**, 2734–2755 (2003).
25. Dash, R. K., Qi, F. & Beard, D. A. A biophysically based mathematical model for the kinetics of mitochondrial calcium uniporter. *Biophys. J.* **96**, 1318–1332 (2009).
26. Marhl, M., Haberichter, T., Brumen, M. & Heinrich, R. Complex calcium oscillations and the role of mitochondria and cytosolic proteins. *Biosystems* **57**, 75–86 (2000).
27. Fall, C. P & Keizer, J. E. Mitochondrial Modulation of Intracellular Ca^{2+} Signaling. *J. Theor. Biol.* **210**, 151–165 (2001).
28. Ndiaye, D. *et al.* Characterization of the Effect of the Mitochondrial Protein Hint2 on Intracellular Ca^{2+} dynamics. *Biophys. J.* **105**, 1268–1275 (2013).
29. Szopa, P., Dyzma, M. & Kazmierczak, B. Membrane associated complexes in calcium dynamics modelling. *Phys. Biol.* **10**, 035004 (2013).
30. Peglow, M., Niemeyer, B. A., Hoth, M. & Rieger, H. Interplay of channels, pumps and organelle location in calcium microdomain formation. *New J. Phys.* **15**, 055022 (2013).
31. Moreau, B., Nelson, C. & Parekhm, A. B. Biphasic regulation of mitochondrial Ca^{2+} uptake by cytosolic Ca^{2+} concentration. *Curr. Biol.* **16**, 1672–1677 (2006).
32. Tang, S. *et al.* Design and application of a class of sensors to monitor Ca^{2+} dynamics in high Ca^{2+} concentration cellular compartments. *Proc. Nat. Acad. Sci.USA* **108**, 16265–16270 (2011).
33. Csordás, G. *et al.* MICU1 Controls Both the Threshold and Cooperative Activation of the Mitochondrial Ca^{2+} Uniporter. *Cell Metab.* **17**, 976–987 (2013).
34. McCarron, J. G., Olson, M. L. & Chalmers, S. Mitochondrial regulation of cytosolic Ca^{2+} signals in smooth muscle. *Pflügers Arch.,-EJP* **464**, 51–62 (2012).
35. Gunter, T. E. & Sheu, S. S. Characteristics and possible functions of mitochondrial Ca^{2+} transport mechanisms. *BBA-Bioenergetics* **1787**, 1291–1308 (2009).
36. Mallilankaraman, K. *et al.* MICU1 Is an Essential Gatekeeper for MCU-Mediated Mitochondrial Ca^{2+} Uptake that Regulates Cell Survival. *Cell* **151**, 630–644 (2012).
37. Baughman, J. M. *et al.* Integrative genomics identifies MCU as an essential component of the mitochondrial calcium uniporter. *Nature* **476**, 341–345 (2011).
38. De Stefani, D., Raffaello, A., Teardo, E., Szabò, I. & Rizzuto, R. A forty-kilodalton protein of the inner membrane is the mitochondrial calcium uniporter. *Nature* **476**, 336–340 (2011).
39. Raffaello, A. *et al.* The mitochondrial calcium uniporter is a multimer that can include a dominant-negative pore-forming subunit. *EMBO J.* **32**, 2362–2376 (2013).
40. Csordás, G., Thomas, A. P. & Hajnóczky, G. Quasi-synaptic calcium signal transmission between endoplasmic reticulum and mitochondria. *EMBO J.* **18**, 96–108 (1999).
41. Taufiq-Ur-Rahman, A. S., Falcke, M. & Taylor, C. W. Clustering of $InsP_3$ receptors by $InsP_3$ retunes their regulation by $InsP_3$ and Ca^{2+}. *Nature* **458**, 655–659 (2009).
42. Dickinson, G. D., Swaminathan, D. & Parker, I. The probability of triggering calcium puffs is linearly related to the number of inositol trisphosphate receptors in a cluster. *Biophys. J.* **102**, 1826–1836 (2012).
43. Vais, H., Foskett, J. K. & Mak, D.-O. D. Unitary Ca^{2+} current through recombinant type 3 InsP3 receptor channels under physiological ionic conditions. *J. Gen. Physiol.* **136**, 687–700 (2010).
44. Smith, G. D. Analytical steady-state solution to the rapid buffering approximation near an open Ca^{2+} channel. *Biophys. J.* **71**, 3064–3072 (1996).
45. Neher, E. Vesicle Pools and Ca^{2+} Microdomains: New Tools for Understanding Their Roles in Neurotransmitter Release. *Neuron* **20**, 389–399 (1998).
46. Arnaudeau, S., Kelley, W. L., Walsh, J. V. & Demaurex, N. Mitochondria recycle Ca^{2+} to the endoplasmic reticulum and prevent the depletion of neighboring endoplasmic reticulum regions. *J. Biol. Chem.* **276**, 29430–29439 (2001).
47. Ishii, K., Hirose, K. & Iino, M. Ca^{2+} shuttling between endoplasmic reticulum and mitochondria underlying Ca^{2+} oscillations. *EMBO Rep.* **7**, 390–396 (2006).
48. Kornmann, B. The molecular hug between the ER and the mitochondria. *Curr. Opin. Cell Biol.* **25**, 1–6 (2013).
49. Berridge, M. J. Calcium oscillations. *J. Biol. Chem.* **265**, 9583–9586 (1990).
50. Camacho, P. & Lechleiter, J. D. Increased frequency of calcium waves in *Xenopus laevis oocytes* that express a calcium-ATPase. *Science* **260**, 226–229 (1993).
51. Kim, I., Xu, W. J. & Reed, J. C. Cell death and endoplasmic reticulum stress: disease relevance and therapeutic opportunities. *Nat. Rev. Drug Discov.* **7**, 1013–1030 (2008).
52. Kaftan, E. J., Xu, T., Abercrombie, R. F. & Hille, B. Mitochondria shape hormonally induced cytoplasmic calcium oscillations and modulate exocytosis. *J. Biol. Chem.* **275**, 25465–25470 (2000).
53. Pacher, P., Csordás, G., Schneider, T. G. & Hajnóczky, G. Quantification of calcium signal transmission from sarco-endoplasmic reticulum to the mitochondria. *Journal Physiol.* **529**, 553–564 (2000).
54. Wang, X. & Schwarz, T. L. The Mechanism of Ca^{2+}-Dependent Regulation of Kinesin-Mediated Mitochondrial Motility. *Cell* **136**, 163–174 (2009).
55. Friedman, J. R., Lackner, L. L, West, M., DiBenedetto, J. R., Nunnari, J. & Voeltz, G. K. ER tubules mark sites of mitochondrial division. *Science* **334**, 358–362 (2011).
56. Walther, P., Höhn, K. & Krisp, H. What is the true size of the mitochondrial intermembrane space? A study using high-pressure freezing and STEM tomography. *Proceedings of MC* **2**, 49–50 (2009).
57. Jafri, M. S., Rice, J. J. & Winslow, R. L. Cardiac Ca^{2+} dynamics: The roles of ryanodine receptor adaptation and sarcoplasmic reticulum load. *Biophys. J.* **74**, 1149–1168 (1998).
58. LeBeau, A. P., Van Goor, F., Stojilkovic, S. S. & Sherman A. Modeling of membrane excitability in gonadotropin-releasing hormone-secreting hypothalamic neurons regulated by Ca^{2+} mobilizing and adenylyl cyclase-coupled receptors. *J. Neurosci.* **20**, 9290–9297 (2000).
59. Higgins, E. R. *et al.* Modelling calcium microdomains using homogenisation. *J. Theor. Biol.* **247**, 623–644 (2007).

60. Means, S. A. & Sneyd, J. Spatio-temporal calcium dynamics in pacemaking units of the interstitial cells of Cajal. *J. Theor. Biol.* **267**, 137–152 (2010).

Acknowledgments

We would like to acknowledge many useful conversations with George Dickinson, Ian Parker and Jeffery Lock in University of California, Irvine. We also thank Ke Jiang and Yu Jiang in Xiamen University for help with numerical simulations. This work was supported by the China National Funds for Distinguished Young Scholars under grant 11125419, the National Natural Science Foundation of China under grant 31370830, the Fujian Province Funds for Leading Scientist in Universities and ICAM branches cost sharing fund.

Author contributions

H.Q. and J.S. conceived and designed the model. H.Q. performed the numerical simulations. L.L. contributed to the writing of the programs. H.Q. and J.S. wrote the paper.

Additional information

Supplementary information accompanies this paper at http://www.nature.com/scientificreports

Competing financial interests: The authors declare no competing financial interests.

How to cite this article: Qi, H., Li, L. & Shuai, J. Optimal microdomain crosstalk between endoplasmic reticulum and mitochondria for Ca^{2+} oscillations. *Sci. Rep.* **5**, 7984; DOI:10.1038/srep07984 (2015).

This work is licensed under a Creative Commons Attribution-NonCommercial-NoDerivs 4.0 International License. The images or other third party material in this article are included in the article's Creative Commons license, unless indicated otherwise in the credit line; if the material is not included under the Creative Commons license, users will need to obtain permission from the license holder in order to reproduce the material. To view a copy of this license, visit http://creativecommons.org/licenses/by-nc-nd/4.0/